Nonisothermal Crystallization Kinetics and Morphology of Poly(ethylene terephthalate) Modified with Poly(lactic acid)

Işıl Acar, Ali Durmuş, Saadet Özgümüş

Department of Chemical Engineering, Faculty of Engineering, Istanbul University, 34320, Avcilar, Istanbul, Turkey

Received 4 October 2006; accepted 3 June 2007
DOI 10.1002/app.26982
Published online 7 September 2007 in Wiley InterScience (www.interscience.wiley.com).

ABSTRACT: The nonisothermal crystallization kinetics of poly(ethylene terephthalate) (PET) copolymers modified with poly(lactic acid) (PLA) were investigated with differential scanning calorimetry, and a crystal morphology of the samples was observed with scanning electron microscopy. Waste PET (P100) obtained from postconsumer water bottles was modified with a low-molecular-weight PLA. The PET/PLA weight ratio was 90/10 (P90) or 50/50 (P50) in the modified samples. The nonisothermal melt-crystallization kinetics of the modified samples were compared with those of P100. The segmented block copolymer structure (PET-*b*-PLA-*b*-PET) of the modified samples formed by a transesterification reaction between the PLA and PET units in solution and the length of the aliphatic and aromatic blocks were found to have a great effect on the nucleation mechanism and overall crystallization rate. On the basis of the results of the crystallization kinetics determined by several models (Ozawa, Avrami, Jeziorny, and Liu–Mo) and morphological observations, the crystallization rate of the samples decreased in the order of P50 > P90 > P100, depending on the amount of PLA in the copolymer structure. However, the apparent crystallization activation energies of the samples decreased in the order of P90 > P100 > P50. It was concluded that the nucleation rate and mechanism were affected significantly by the incorporation of PLA into the copolymer structure and that these also had an effect on the overall crystallization energy barrier. © 2007 Wiley Periodicals, Inc. J Appl Polym Sci 106: 4180–4191, 2007

Key words: crystallization; DSC; biodegradable; polyesters; morphology

INTRODUCTION

Poly(ethylene terephthalate) (PET) is the most widely used semicrystalline thermoplastic polyester in many areas in the plastic industry, such as fibers, packaging films, food and beverage bottles, containers for pharmaceutical and household products, and cosmetics, because of its superior thermal and mechanical properties, low permeability, and chemical resistance.

As the amount of PET in waste plastic feedstock has increased, recycling has become more crucial from an ecological point of view. Nowadays, ecological and economic considerations have led to research studies focusing on the chemical recycling of waste PET. One of the recent solutions is to prepare biodegradable PET materials by chemical modification reactions, reactive blending, or copolymerization.

PET shows interesting thermal and crystallization characteristics. It can be quenched into the amorphous state or crystallized from the melt state by cooling (melt crystallization) over a wide range of supercooling conditions depending on the thermomechanical history and structural properties. It can also be crystallized from the solid–amorphous (glassy) state through heating (cold crystallization) above the glass-transition temperature (T_g).[1] PET has a slow crystallization rate (the maximum radial growth rate of PET has been reported to be 10 μm/min) in the melt-crystallization process with respect to its chemical structure in comparison with other semicrystalline polyesters such as poly(butylene terephthalate), poly(trimethylene terephthalate), and thermoplastics (e.g., the radial growth rate of polyethylene is ca. 5000 μm/min).[2–5] Thus, the injection-molding applications of PET are rather limited in engineering applications and require a large cycle time. Some studies have been reported about the crystallization kinetics of virgin or recycled PET compounded with special additives, nucleating agents, crystallization promoters, and so forth.[6–9] In PET processing, the most widely used nucleating agent is talc. It is also well known that some other compounds and additives such as metal oxides, ionomers, and fibers show nucleating ability for PET. Besides the physical effects of additives on the crystallization rate of PET due to their crystallization rate enhancement ability, the effects of chemical modifications by copolymerization or blending with other polymers on the crystallization behavior of PET have been investigated.[10–17]

Correspondence to: I. Acar (acar@istanbul.edu.tr).

Journal of Applied Polymer Science, Vol. 106, 4180–4191 (2007)

Agarwal et al.[16] reported that the solid-state chemical modification of PET enhanced the crystallization rate significantly.[16] They modified commercial-grade PET pellets in the solid state by directly exposing them to vapors of a reactive functional monomer, ethylenediamine (EDA), in a simple glass flask at 125°C under a vacuum. Then, they homogenized the modified PET pellets through melt processing in a twin-screw miniextruder. They showed that the reaction with EDA caused the incorporation of amide segments into the PET structure and enhanced the crystallization rate according to the differential scanning calorimetry (DSC) analysis.

Poly(lactic acid) (PLA) is a linear aliphatic thermoplastic polyester that is a slower crystallizing polymer and shows crystallization behavior very similar to that of PET.[18] Recently, it has become the most common and promising green polymer in various applications because of its biodegradability. Generally, it yields an amorphous structure at high cooling rates and forms a spherulitic crystalline morphology at very low cooling rates. Thus, its processability is not good for industrial processing operations in the case of a homopolymer structure. On the other hand, PLA shows cold-crystallization behavior depending on the thermal conditions.

In this study, the nonisothermal crystallization kinetics of biodegradable PET copolymers prepared by the modification of waste PET with low-molecular-weight PLA were investigated with DSC. To the best of our knowledge, PET–PLA copolymers were prepared by the chemical modification of waste PET in a solution phase for the first time. Crystallization kinetics of the samples were determined with the Ozawa, Avrami, and Lui–Mo models, and the crystallization rates of the modified samples were compared. The apparent activation energy of the overall crystallization process was also calculated with the Kissinger method. The availability of the modified products for the injection-molding operations is discussed on the basis of the crystallization rates of the samples under nonisothermal conditions.

EXPERIMENTAL

Materials

The modified PET products employed in this study were prepared in solution, and the experimental details of the preparation reactions, chemical characterization of the modified samples by Fourier transform infrared (FTIR) and DSC, and hydrolytic decomposition results were reported previously.[19] The biodegradability and hydrolytic decomposition behavior of the samples prepared with a very wide range of compositions and by different reaction conditions were also reported in detail previously.[20] The viscosity-average molecular weight of the waste PET obtained from water bottles and the number-average molecular weight of the oligomeric PLA synthesized in the laboratory were 3.7×10^{4} [21] and 2.6×10^{3} g/mol,[19] respectively. The samples used in this study are called P100, P90, and P50, which indicate the weights of PET in the initial polymer mixtures as percentages: 100 PET/0 PLA, 90 PET/10 PLA, and 50 PET/50 PLA, respectively. P100 consisted of 2–0.85 mesh waste PET flakes obtained by grinding of wastewater bottles. PLA-modified samples were also ground into similar size flakes.

DSC study

Before the DSC runs, all samples were dried well at 40°C in a vacuum oven at the pressure of 100 mbar overnight. Melting and crystallization runs were carried out with a Setaram DSC-131 (Caluire, France). The temperature and heat flow calibration of the instrument were achieved with high-purity indium, zinc, and copper metals. In the first runs, samples weighing about 5– 8 mg in an aluminum crucible were heated from room temperature to 310°C at a heating rate of 20°C/min. The samples were isothermally kept at this temperature for 5 min to eliminate the thermal history and unmelted crystals that could cause heterogeneous nucleation. Then, they were cooled to 20°C with a liquid-nitrogen cooling device at a constant cooling rate, and the crystallization exotherms were recorded to investigate the crystallization kinetics of the PET and modified PET samples. The cooling rates employed in this study were 1.5, 3, 5, 7.5, and 10°C/min. Relatively low cooling rates were preferred to complete the crystallization process of the samples as much as possible. All melting and crystallization experiments were carried out under a nitrogen (N_2) atmosphere at a flow rate of 100 mL/min to prevent the thermal degradation of the samples. After the completion of the crystallization process during the first heating–cooling run, the samples were kept at 20°C for 5 min. Subsequently, the nonisothermally crystallized samples at different cooling rates were heated again from 20 to 310°C at a heating rate of 10°C/min. Second heating runs were used to characterize the melting behavior and determine the melting enthalpy [ΔH_m (J/g)] of the samples, which depended on the sample composition and dynamic crystallization conditions.

Scanning electron microscopy (SEM) study

A JEOL JSM-5600 scanning electron microscope (Tokyo, Japan) (acceleration voltage = 15 kV) was used to examine the morphology of the PET and PET–PLA copolymers. Samples crystallized at different cooling

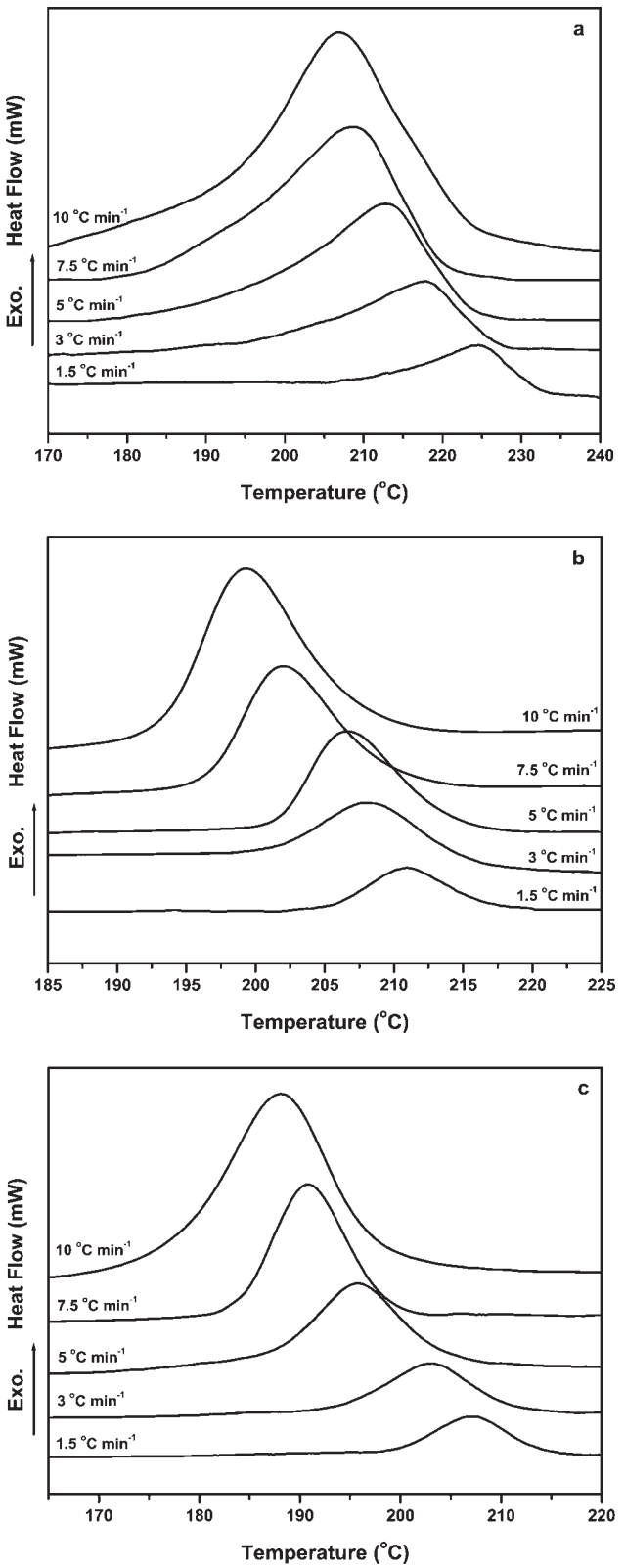

Figure 1 Crystallization exotherms of samples (a) P100, (b) P90, and (c) P50.

rates in a DSC crucible were directly imaged with a magnification of 1000× by SEM without any surface treatment (washing, etching, etc.) over the samples.

RESULTS AND DISCUSSION

Nonisothermal crystallization kinetics

The crystallization exotherms of samples P100, P90, and P50 at various cooling rates are illustrated in Figure 1(a–c), respectively. As shown in Figure 1, the modified samples crystallize in relatively narrow temperature ranges in comparison with the temperature range of PET crystallization at all cooling rates employed. In addition to this behavior, it can also be clearly seen that the crystallization exotherms of PET show a secondary crystallization region that is characteristic of the PET crystallization process at low temperatures. The crystallization peak temperatures (T_c's) of the samples at which the crystallization rate is maximum at all cooling rates are listed in Table I. As expected, the T_c values shift to lower temperatures with an increasing cooling rate for all the samples. P90 and P50 show only a single crystallization peak at all cooling rates. In the first and second heating runs of P90 and P50, no peak can be observed at the temperatures around the melting temperature (T_m) of the PLA ($\sim$ 140°C) synthesized and used in this study. These single crystallization peaks can be attributed to the cocrystallization behavior of the PLA and PET blocks and also confirm the reaction between these units. However, the incorporation of PLA units affects the crystallization behavior of PET; we have deduced that PLA units enter the crystal lattice as a result of the formation of an AAAB-BAAA-type segmented block copolymer by transesterification reactions between the PET and PLA units. The structure of the segmented block copolymer is schematized in Scheme 1. This structure has also been characterized with an FTIR study of the modified samples; absorption bands have been observed at 1750 cm^{-1}, which indicates the O—CO and C=O bonds, and at 1456 cm^{-1}, which indicates CH_3 groups of the PLA units, which have been reported previously.[18] These results indicate that transesterification reactions occur between the PET and PLA units and that a segmented block copolymer structure has formed. For a given cooling rate, the onset and peak maximum temperatures of the crystallization decrease in the order of P100 > P90 > P50. This decrease shows that PLA incorporation into the PET structure reduces the nucleation ability

TABLE I
T_c Values of the Samples

	Cooling rate (°C/min)				
Sample	1.5	3	5	7.5	10
P100	224.5	217.8	212.8	208.7	206.8
P90	210.9	208.0	206.6	202.0	199.3
P50	207.3	203.2	195.7	190.8	188.1

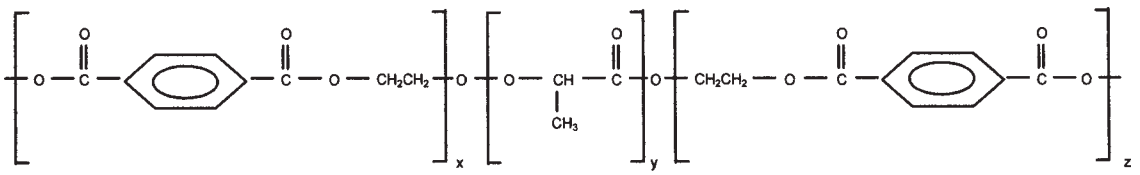

Scheme 1 Structure of the PET-*b*-PLA-*b*-PET segmented block copolymer.

of PET chains. It is well known that the thermally induced nucleation of PET originates from hydrogen bonding between the aromatic groups on the main backbone. In general, the chemical modification of PET by the incorporation of secondary units (copolymerization, reactive blending, etc.) changes the crystallization behavior as well as its other physical and thermal properties.[1] Some authors have indicated that random branching decreases the crystallization rate; however, a low branch content could accelerate the nucleation.[22] Some studies have also shown that ionic end groups (e.g., ionomers) can cause chemical nucleation for PET because of strong electrostatic interactions and cluster formation, which reduces the chain mobility and facilitates the formation of stable nuclei.[23,24] We have deduced that the effect of the PLA units on the nucleation is quite different from classical heterogeneous nucleation, which is achieved by nucleating agents, and chemical nucleation, which results from chain modification by ionic groups. We have concluded that when the amount of PLA increases in the sample composition, the number of PLA units in the PET-*b*-PLA-*b*-PET structure or length of the PLA segments along the copolymer structure also increases. On the other hand, PLA units can be called soft segments in the copolymer structure. These PLA blocks must have higher mobility than PET blocks at the crystallization temperatures because of the relatively low T_g value of PLA. We have speculated that such a decrease in the crystallization onset and peak temperatures originates from the higher mobility of soft PLA segments. Several authors have studied the crystallization kinetics of PET copolymers, using different comonomers with various properties, and reported similar behaviors for the crystallization of PET copolymers. Kong and coworkers[12,13] investigated the isothermal and nonisothermal crystallization kinetics of PET–poly(ethylene oxide) (PEO) segmented copolymers with two crystallizing blocks and reported that the crystallization behavior of the copolymer was strongly influenced by the presence of comonomer units. They also showed that the isothermal crystallization rate of PET blocks in the copolymer was faster than that of the pure PET homopolymer because of the lower T_g value of the soft blocks (PEO), which increased the mobility of the PET blocks in the copolymer.[14] Xiao et al.[15] studied the crystallization kinetics of copoly(ethylene terephthalate imide)s under isothermal and nonisothermal conditions. The authors reported that both isothermal and nonisothermal crystallization rates of the copolymers increased first and then decreased as the content of imide units in the copolymer increased. Zhang and Gu[17] examined the nonisothermal crystallization kinetics of poly(ethylene terephthalate-*co*-isophthalate) and revealed that the crystallization mechanism of the copolymers differed, depending on the sequence length and distribution of the isophthalate units in the copolymer structure. Bouma et al.[25] studied the physical and thermal properties of poly(ester amide)s based on PET and nylon 2 and reported similar behavior—an increase in the crystallization rate of the modified samples with the incorporation of diamide segments into the PET structure—for the crystallization rates of the poly(ester amide)s. Our results indicate similar trends for the crystallization behavior of PET–PLA copolymers. It can be said that these results are very consistent with the reported studies on the crystallization behavior of PET copolymers. Furthermore, crystallization rates of the modified samples, P90 and P50, are discussed in this article, and the kinetic results are compared with the crystallization rate of the waste PET, P100.

The relative crystallinity (X_c) as a function of the crystallization temperature and time can be obtained from the crystallization exotherms of samples by partial integration of the crystallization exotherms. X_c as a function of the crystallization temperature can be defined as follows:

$$\chi_c = \frac{\int_{T_o}^{T} \left(\frac{dH_c}{dT}\right) dT}{\int_{T_o}^{T_\infty} \left(\frac{dH_c}{dT}\right) dT} \quad (1)$$

where T_o and T represent the onset and end temperatures of the crystallization, respectively. X_c–temperature curves of the P100, P90, and P50 samples are presented in Figure 2(a–c), respectively. Figure 3(a–c) shows X_c of the samples versus time. All X_c–temperature curves at various cooling rates have the same characteristic sigmoidal shape, which implies the lag effect of cooling on the crystallization pro-

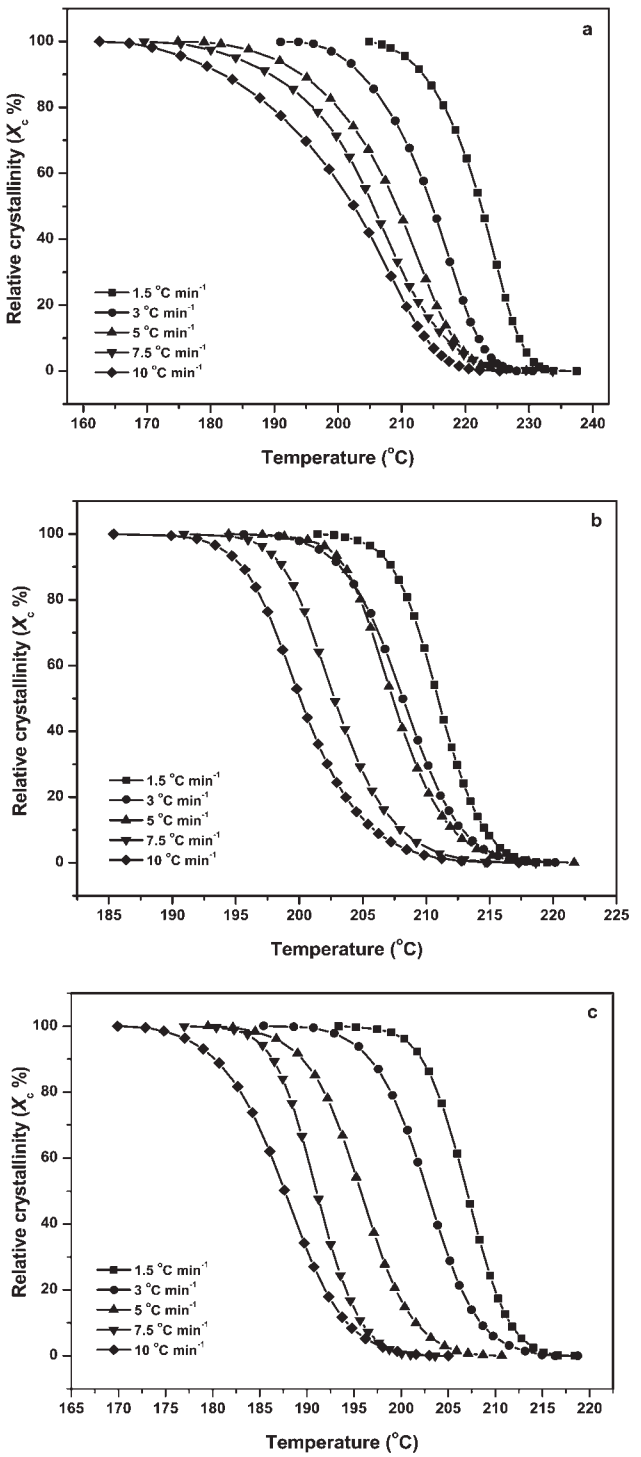

Figure 2 X_c as a function of temperature at five different cooling rates for samples (a) P100, (b) P90, and (c) P50.

cess. First, the nonlinear, initial part of the S-shaped curves is generally considered the nucleation step of the crystallization process. Each curve shows a linear part considered to be due to primary crystallization; subsequently, a second nonlinear part deviates slightly and is considered to be due to secondary crystallization, which is caused by spherulite impingement in a further step of crystal growth. For the X_c–time curves, the higher cooling rate means a shorter time to complete the crystallization. The most important rate parameter, the crystallization half-time ($t_{1/2}$), which is defined as the time needed for the crystallinity of a sample to reach a value that

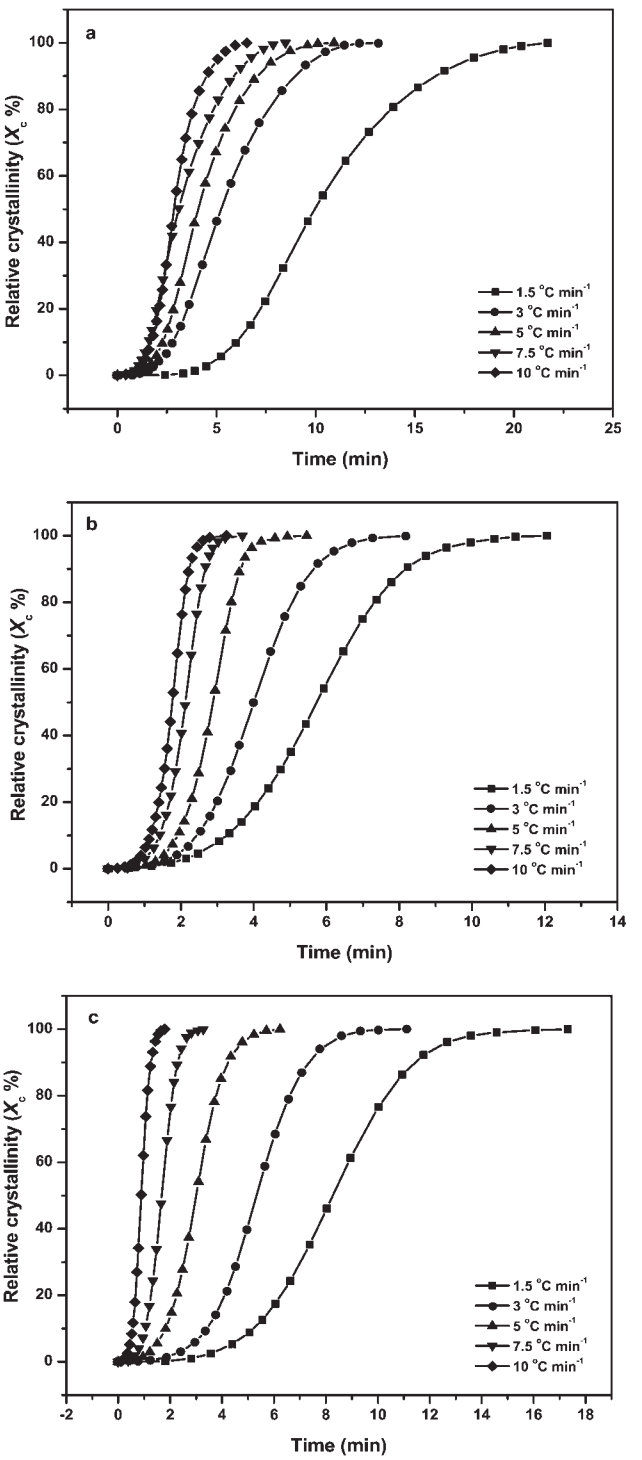

Figure 3 X_c as a function of time at five different cooling rates for samples (a) P100, (b) P90, and (c) P50.

TABLE II
Crystallization Rate Parameters

Sample		Cooling rate (°C/min)				
		1.5	3	5	7.5	10
P100	$t_{1/2}$ (min)	9.97	5.23	4.11	3.07	2.84
	$1/t_{1/2}$ (min^{-1})	0.10	0.19	0.24	0.33	0.35
P90	$t_{1/2}$ (min)	5.73	4.02	2.89	2.12	1.75
	$1/t_{1/2}$ (min^{-1})	0.18	0.25	0.35	0.47	0.57
P50	$t_{1/2}$ (min)	8.28	5.32	2.99	1.69	0.87
	$1/t_{1/2}$ (min^{-1})	0.12	0.19	0.33	0.59	1.14

is 50% of X_c, can be obtained from the X_c–time curves. $t_{1/2}$ directly indicates the rate of the crystallization process, and usually the reciprocal of the crystallization half-time ($1/t_{1/2}$) is used to compare crystallization rates of different systems. If $t_{1/2}$ is short or its reciprocal time is high, the crystallization is fast.

The $t_{1/2}$ and $1/t_{1/2}$ values of the samples are given in Table II. As expected, the $t_{1/2}$ values decrease with an increase in the cooling rate for all samples. Curves of $1/t_{1/2}$ versus the cooling rate of the samples are also plotted in Figure 4. As shown, the crystallization rates increase with increases in the cooling rate for the samples. P100 has the lowest crystallization rate at a given cooling rate. Comparing the $1/t_{1/2}$ values of the modified samples, we see that the crystallization rate of P90 is higher than that of P50 at low cooling rates (<5°C/min). On the other hand, P50 crystallizes much faster than P90 at relatively high cooling rates (>5°C/min). This increase in the crystallization rate with an increasing number of PLA units in the copolymer structure can be attributed to the fact that chain diffusion toward the growing crystal face and packaging are dominant processes at especially high cooling rates. We have deduced that increasing the number of PLA units in the copolymer structure increases the rate of crystal growth on the nascent PET crystals, which are nucleated earlier than the PLA segments.

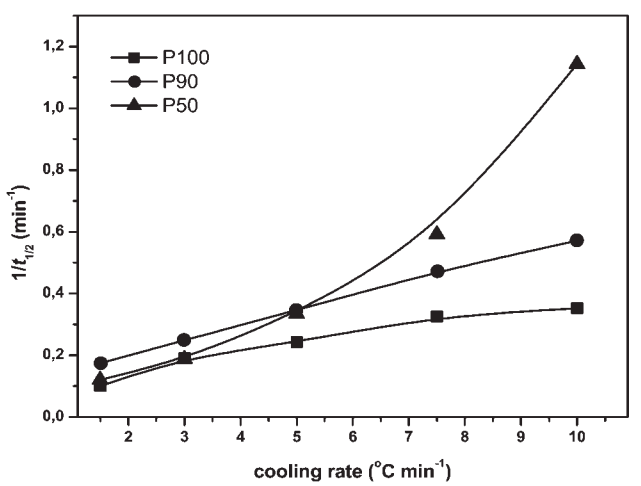

Figure 4 $1/t_{1/2}$ versus the cooling rate.

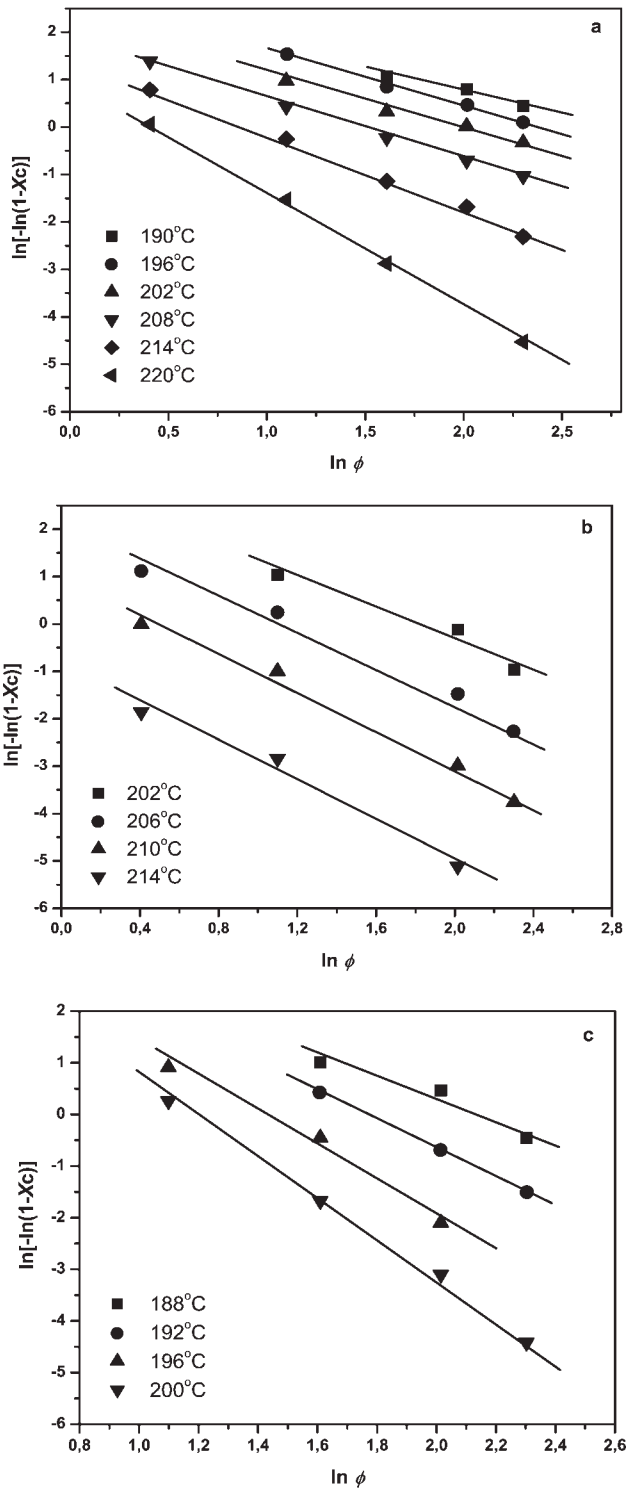

Figure 5 Ozawa plots {ln[−ln(1 − X_c)] vs ln φ} of samples (a) P100, (b) P90, and (c) P50.

The most used kinetic approach for the nonisothermal crystallization process of polymers is the Ozawa model.[26] It is based on the extended form of

TABLE III
Ozawa Kinetic Parameters

Sample	Temperature (°C)	m	$K(T)$ [(°C/min)^m]	r^2
P100	190	0.87	2.498	0.985
	196	1.17	2.809	0.997
	202	1.05	2.101	0.995
	208	1.28	1.871	0.999
	214	1.61	1.468	0.999
	220	2.43	1.072	0.999
P90	202	1.56	2.804	0.979
	206	1.77	1.978	0.992
	210	1.98	0.956	0.994
	214	2.05	0.864	0.989
P50	188	2.05	4.392	0.971
	192	2.80	4.954	0.999
	196	3.48	4.869	0.988
	200	3.89	4.553	0.999

an Avrami approximation assuming that the nonisothermal crystallization process can be divided into small isothermal steps. The Ozawa equation is as follows:

$$\chi_c = 1 - \exp\left(\frac{-K(T)}{\Phi^m}\right) \quad (2)$$

where $K(T)$ is the cooling function, Φ is the cooling/heating rate (°C/min), and m is the Ozawa constant depending on the dimension of crystal growth and the nucleation mechanism. If the double logarithmic form of the equation is taken, a linear relationship is obtained to calculate kinetic constants:

$$\ln[-\ln(1-\chi_c)] = \ln\ K(T) - m\ln\Phi \quad (3)$$

Plotting $\ln[-\ln(1-\chi_c)]$ against $\ln\Phi$ at a given temperature, we should obtain a straight line. The slope of the line is m, and the intercept is $K(T)$. Ozawa plots of the samples are given in Figure 5(a–c) for P100, P90, and P50, respectively. As shown in Figure 5, the Ozawa model successfully fits the nonisothermal crystallization behavior of the samples. Some authors have claimed that the Ozawa model cannot be used for modeling the crystallization kinetics of polymers that have secondary crystallization.[27,28] We have found that our results follow well the Ozawa model for the nonisothermal crystallization of modified PET samples. The Ozawa kinetic parameters are listed in Table III. m increases as the crystallization temperature increases. Interestingly, higher m values have been obtained for the P50 sample than for both P90 and P100, although T_c decreases in the order of P100 > P90 > P50. Similarly, the m values of P90 are higher than those of P100. This relationship between the sample composition and m values shows that the incorporation of PLA into the copolymer structure results in crystal perfection and three-dimensional growth. The $K(T)$ values given in Table III imply that the crystallization rate function decreases when the temperature increases for a particular sample. On the other hand, at a given crystallization temperature (e.g., at 202°C for P100 and P90 and at 200°C for P50), the $K(T)$ values decrease in the order of P50 > P90 > P100. This result indicates that the crystallization rate increases with an increasing number of PLA units in the copolymer structure.

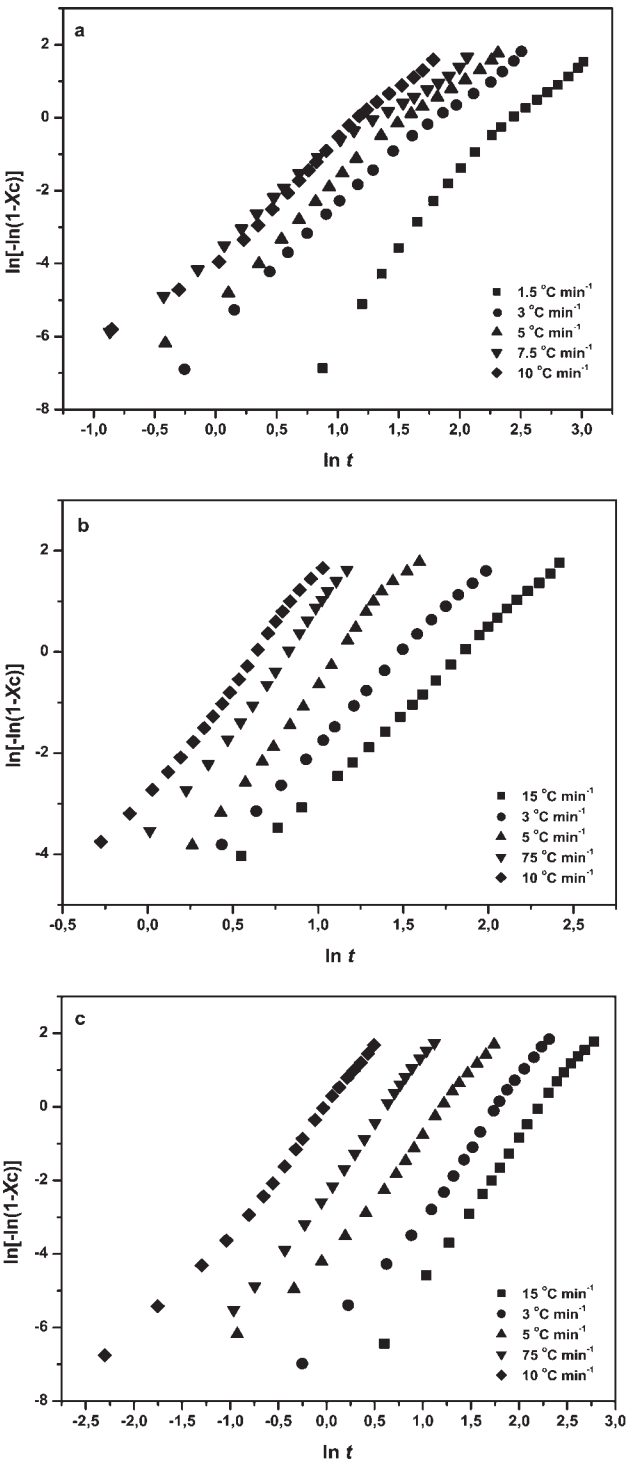

Figure 6 Avrami plots $\{\ln[-\ln(1 - X_c)]$ vs $\ln t\}$ of samples (a) P100, (b) P90, and (c) P50.

TABLE IV
Avrami and Modified Avrami (Jeziorny) Kinetic Parameters

	P100			P90			P50		
Cooling rate (°C/min)	n	Z_c (min^{-1})	r^2	n	Z_c (min^{-1})	r^2	n	Z_c (min^{-1})	r^2
1.5	4.36	0.002	0.988	3.20	0.026	0.999	3.83	0.003	0.999
3	3.29	0.147	0.996	3.59	0.183	0.999	3.56	0.119	0.998
5	3.22	0.369	0.996	4.47	0.384	0.998	3.15	0.461	0.995
7.5	2.80	0.620	0.996	4.67	0.628	0.998	3.62	0.740	0.999
10	3.06	0.671	0.995	4.42	0.784	0.997	3.16	0.997	0.995

An alternative approach, the Avrami model,[29–31] was used in this study to compare the crystallization rates of the samples. The Avrami equation is as follows:

$$\chi_c = 1 - \exp(-Z_t t^n) \tag{4}$$

where n is the Avrami constant depending on the crystal growth mechanism, t is the time, and Z_t is the rate constant involving both nucleation and growth rate parameters. The double logarithmic form of the equation is

$$\ln[-\ln(1 - \chi_c)] = \ln Z_t + n \ln t \tag{5}$$

Plotting $\ln[-\ln(1 - \chi_c)]$ versus $\ln t$ for each cooling rate, we should obtain a straight line to determine the kinetic constants. Avrami plots generally fit the experimental data linearly at a low degree of crystallinity and deviate from the linear regression at a higher crystallization ratio because it possibly does not account for secondary crystallization. In nonisothermal crystallization, a temperature change at a given constant cooling rate affects the rates of both nucleation and spherulite growth, which are temperature-dependent parameters. Considering the temperature-dependent character of the nonisothermal crystallization process, Jeziorny[32] modified rate parameter Z_t:

$$\ln Z_c = \frac{\ln Z_t}{\Phi} \tag{6}$$

where Z_c is the cooling rate independent rate constant. Avrami plots of the samples are illustrated in Figure 6, and the kinetic constants by the Jeziorny method are summarized in Table IV. As shown in Figure 6, the Avrami model can fit the primary crystallization stage of the samples, and it deviates from the linearity for secondary crystallization at all cooling rates. Changes in n with the cooling rate imply that crystallization of the samples has occurred in various growth forms. n is in the range of 2.80–4.36 for P100 and decreases as the cooling rate increases. This result shows that the nucleation of PET could be homogeneous and thermally induced at all cooling rates. On the other hand, the crystallization process of PET develops three-dimensional spherulitic

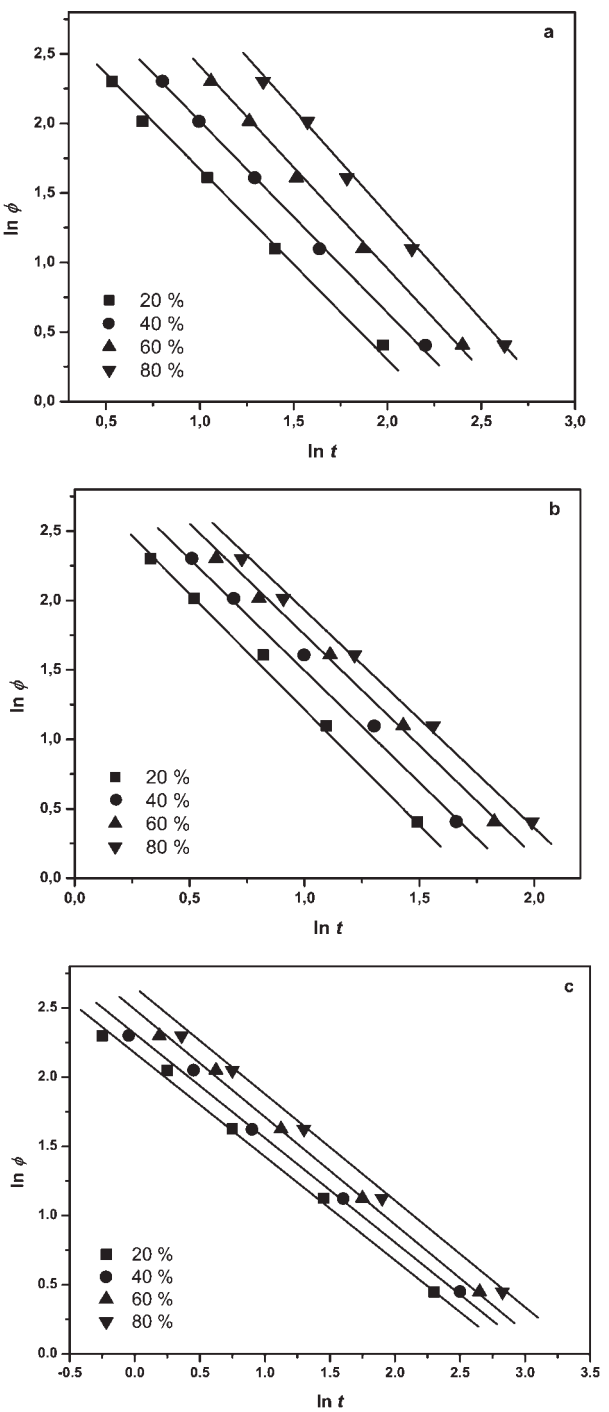

Figure 7 Liu–Mo plots (ln ϕ vs ln t) at different X_c values for samples (a) P100, (b) P90, and (c) P50.

TABLE V
Liu–Mo Kinetic Parameters

Sample	X_c (%)	a	$F(T)$	r^2
P100	80	1.50	4.31	0.998
	60	1.42	3.79	0.999
	40	1.35	3.36	0.999
	20	1.30	2.95	0.999
P90	80	1.49	3.39	0.999
	60	1.55	3.28	0.998
	40	1.62	3.16	0.997
	20	1.63	2.87	0.998
P50	80	0.75	2.54	0.998
	60	0.75	2.40	0.998
	40	0.75	2.28	0.998
	20	0.74	2.14	0.999

growth at low cooling rates. Low cooling rates allow PET to crystallize regularly for a relatively long time. Contrarily, n of the P90 sample increases as the cooling rate increases (between 3.20 and 4.67). Similarly, the n values are in the range of 3.16–3.83 for P50. This result shows that the incorporation of PLA into the copolymer structure causes crystal perfection and three-dimensional, spherulitic crystal growth as well as increases in the crystallization rate.

Another method developed by Liu and Mo was also used to describe the nonisothermal crystallization process. Liu et al.[33] offered a new method combining the Avrami and Ozawa equations at a given value of X_c as follows:

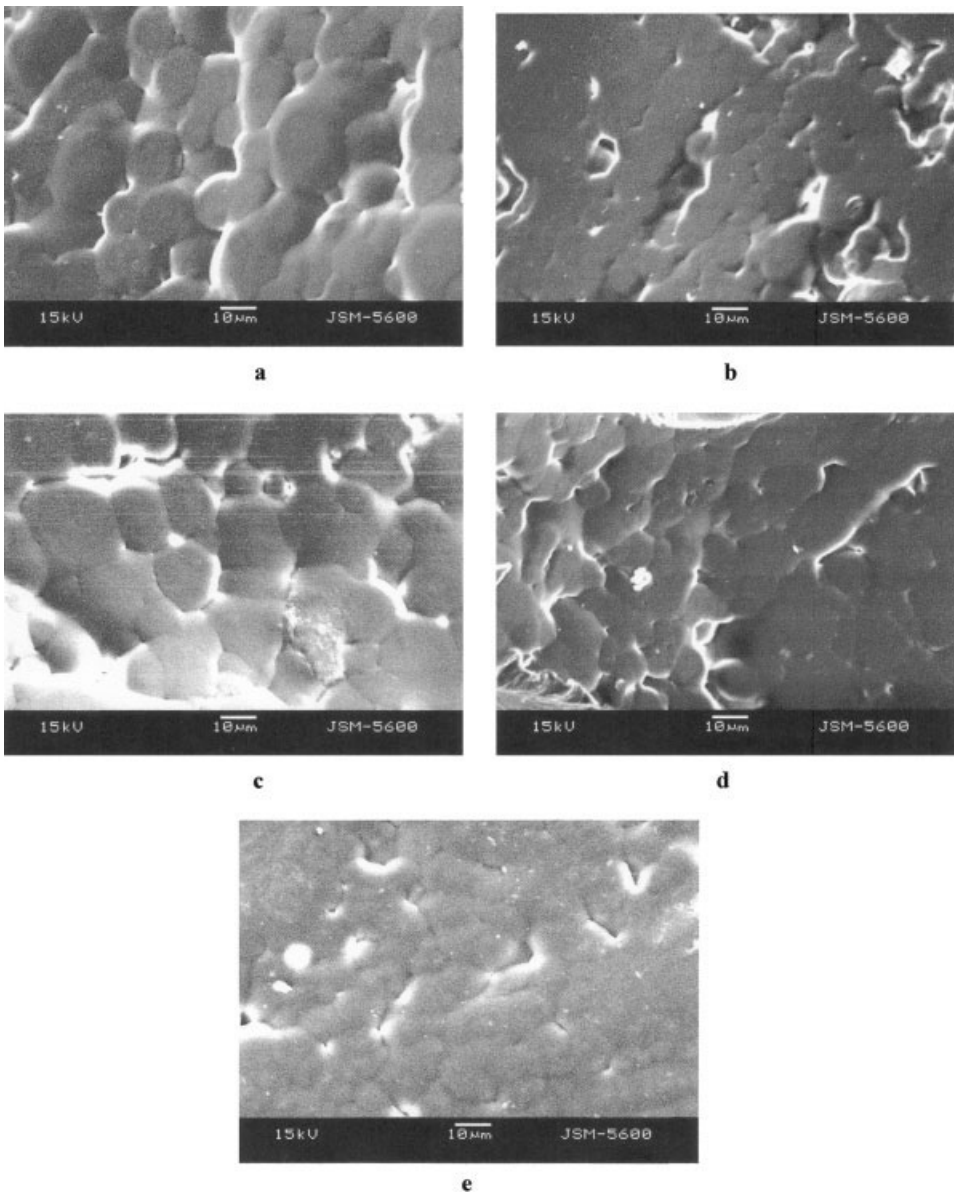

Figure 8 SEM images of samples crystallized at different cooling rates: (a) P50 at 5°C/min, (b) P50 at 10°C/min, (c) P90 at 5°C/min, (d) P90 at 10°C/min, and (e) P100 at 5°C/min.

$$\ln K(T) - m \ln \Phi = \ln Z_t + n \ln t \quad (7)$$

$$\ln \Phi = \ln F(T) - a \ln t \quad (8)$$

where $F(T) = [K(T)/Z_t]^{1/m}$ refers to the cooling rate and a is the ratio of n to m. According to this model, when ln Φ is plotted versus ln t, a series of straight lines are obtained at a given value of X_c. The kinetic parameters, $F(T)$ and a, can be determined from the intercept and slope of these lines, respectively. At a certain value of X_c, a higher value of $F(T)$ means that a high cooling rate is needed to reach X_c in a unit of time, and it also indicates the difficulty of the crystallization process. Liu–Mo plots of the samples are given in Figure 7(a–c) for P100, P90, and P50, respectively. The Liu–Mo model was applied to data at the X_c values of 20, 40, 60, and 80%. Table V summarizes the values of the Liu–Mo parameters for the samples. As shown in Figure 7, the Liu–Mo model successfully fits the crystallization kinetics of the PET and modified PET samples. From the Liu–Mo modeling of the samples, lower $F(T)$ values were obtained for P90 and P50 than P100 at a given X_c value. Similarly, the $F(T)$ values of P50 are lower than those of P90. These results imply that the incorporation of PLA units into the copolymer structure makes the crystallization easier.

Morphology

SEM images of samples crystallized at cooling rates of 5 and 10°C/min are presented in Figure 8. As expected, the average crystal size decreases with an increase in the cooling rate when samples P90 and P50 are compared. The same relationship has been observed for PET (not shown here). On the other hand, the crystal size of P50 and P90 is larger than that of P100 for the cooling rate of 5°C/min. We have concluded that this probably results from the fact that the copolymers have a higher crystal growth rate than PET. Morphological observations depending on the sample composition show that the chain diffusion rate through the growing lamellar face is higher in the copolymers than that in PET in a unit of time for a given cooling rate. As a result of an increasing amount of PLA in the copolymer structure and higher crystal growth rate of the PET-*b*-PLA-*b*-PET segmented block copolymer, larger spherulites are formed.

Crystallization activation energy

In DSC analysis, the activation energy of the crystallization process [E_A (kJ/mol)] can be determined by the Kissinger equation,[34] which considers the variation of T_c (K) with cooling rate Φ (°C/min). The Kissinger equation can be described as follows:

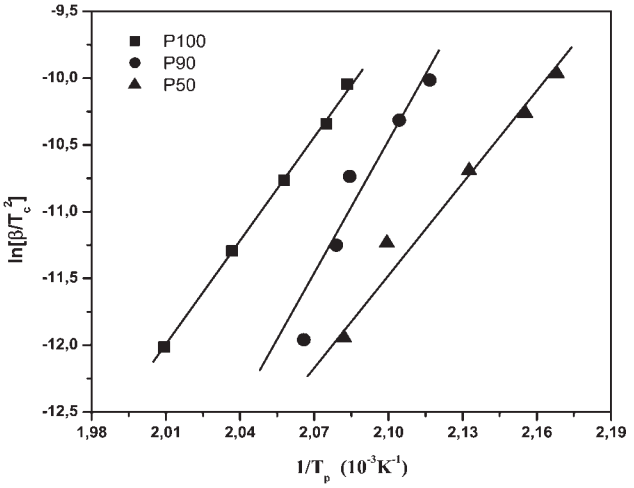

Figure 9 Kissinger plots [ln(β/T_c^2) versus ln($1/T_c$)].

$$\frac{d\left[\ln\left(\frac{\Phi}{T_c^2}\right)\right]}{d\left[\frac{1}{T_c}\right]} = -\frac{E_A}{R} \quad (9)$$

where R is the universal gas constant (8.314 kJ mol^{-1} K^{-1}). When the parameter ln(Φ/T_c^2) is plotted against $1/T_c$, the slope of the curve gives the apparent activation energy of the process. Kissinger plots of the samples are presented in Figure 9. From calculations with the Kissinger model, the activation energies were found to be −217.4 (r^2 = 0.998), −315.0 (r^2 = 0.985), and −177.8 kJ/mol (r^2 = 0.976) for the P100, P90, and P50 samples, respectively. The overall crystallization activation energy is the sum of the activation energies of the nucleation and crystal growth processes. The fact that the P50 sample has the lowest activation energy for the nonisothermal crystallization process shows that the incorporation of PLA into the PET structure also lowers the energy barrier for the crystallization. On the other hand, the E_A value of P90 is higher than those of P100 and P50. This can be explained by the effects of the nucleation mechanism on the crystallization. E_A changes with X_c (or conversion) during the crystallization process, depending on the nucleation mechanism and crystal growth. We have supposed that interactions between the aromatic groups of the PET chains may accelerate the self-nucleation process of PET copolymers and that this effect decreases with an increasing amount of PLA in the copolymer structure. It can be assumed that the nucleation rate of P100 is faster than those of P90 and P50. On the other hand, the incorporation of PLA into the copolymer structure increases the segmental mobility of the copolymer and chain diffusion rate. As the crystal growth is accelerated with the PLA incorporation, the nucleation rate and corresponding nucleation activation energy can be considered the rate-limiting

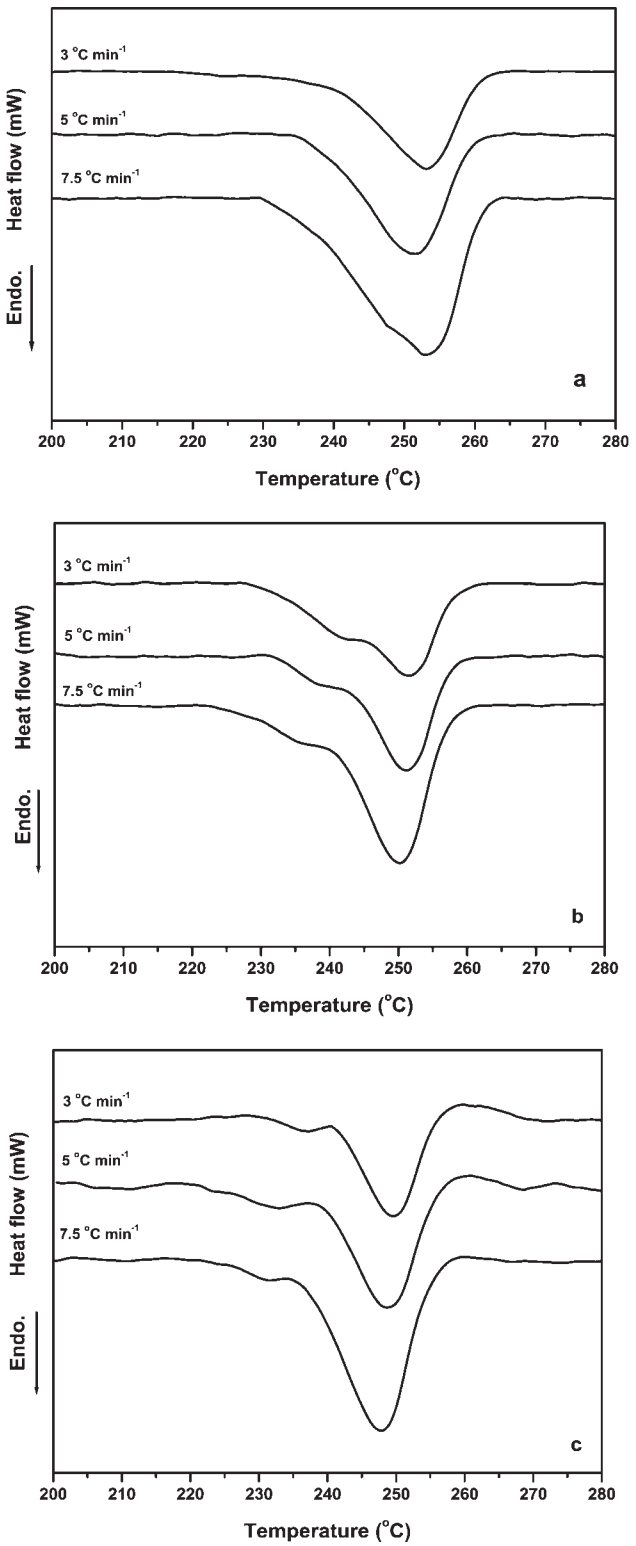

Figure 10 Second melting endotherms of samples (a) P100, (b) P90, and (c) P50 crystallized at different cooling rates.

step for the crystallization. In the case of a low PLA amount (P90), the nucleation activation energy can be higher than that of P100, but the crystal growth activation energy can be higher than that of P50 as 10 wt % PLA cannot enhance the crystal growth rate sufficiently. As a result, the highest E_A value for P90 can be explained if we consider the rate of nucleation and growth steps individually. In this way, these findings on the crystallization activation energy are also consistent with the kinetic results.

Melting behavior

The melting endotherms of samples P100, P90, and P50 crystallized at cooling rates of 3, 5, and 10°C/min are given in Figure 10. The melting endotherms of the samples were recorded during the second run with a heating rate of 10°C/min. In this study, T_m is indicated as the peak maximum temperature of the melting endotherms. T_m and ΔH_m values of the samples are listed in Table VI. The T_m values of P100 (i.e., T_{m2}) are about 251–253°C, depending on the cooling rate. As shown in Figure 10(b,c), small low-temperature melting peaks (T_{m1}) in the melting endotherms of samples P90 and P100 can be observed in the low-temperature region, although these low-temperature melting peaks were not observed for P100. Similar melting behavior and multiple endotherms were reported by several authors for nonisothermally crystallized PET and PET copolymers.[35–38] T_{m1} can be attributed to the effects of the soft blocks on the crystal melting or thinner crystals formed by secondary crystallization. It was observed that the values of the P90 and P50 samples crystallized at a given cooling rate slightly decreased with increasing PLA content in the copolymer structure. As the PLA content increases in the copolymer structure, thinner crystals are formed at lower temperatures because the amount of the soft segment is also increased in the structure. Thus, it can be normally expected that T_{m1} might be observed at lower temperatures, depending on the copolymer composition. On the other hand, the ΔH_m values of the PET and modified samples (P90 and P50) do not change significantly with the cooling rate. However, P50 has a higher ΔH_m value than P100 and P90 at a particular cooling rate. We have concluded that this result also suggests that the degree of crystallinity in the P50 sample could be higher than those of P90 and P100 as well as the crystallization rate.

CONCLUSIONS

We have studied the nonisothermal melt-crystallization kinetics and morphology of PET copolymers prepared through modification reactions of waste PET with low-molecular-weight PLA. The crystallization rates of the samples and related kinetic parameters were analyzed with the Ozawa, Avrami, Jeziorny, and Liu–Mo models. The crystallization activation energies of the samples were determined by the Kissinger method. The incorporation of PLA

TABLE VI
T_m and ΔH_m Values

Cooling rate (°C/min)	P100			P90			P50		
	T_{m1} (°C)	T_{m2} (°C)	ΔH_m (J/g)	T_{m1} (°C)	T_{m2} (°C)	ΔH_m (J/g)	T_{m1} (°C)	T_{m2} (°C)	ΔH_m (J/g)
3	—	253.1	31.3	251.5	243.7	24.6	249.2	239.2	39.9
5	—	251.6	23.6	251.1	240.2	23.0	248.6	233.1	27.9
7.5	—	252.9	28.4	250.2	237.1	30.1	247.8	232.6	37.1

units into the copolymer structure as a result of transesterification reactions between PLA and PET blocks was found to increase the crystallization rate of PET-*b*-PLA-*b*-PET segmented block copolymers on the basis of studies of the crystallization kinetics. This increase is shown more clearly at relatively high cooling rates. PLA incorporation into the crystal lattice results in crystal perfection and three-dimensional growths in the melt-crystallization process. On the basis of the morphological observations of the samples, it can be said that the crystal growth rate or chain diffusion through the growing crystal face increases with the incorporation of PLA units as the soft segment because of its high mobility. We have speculated that biodegradable PET–PLA copolymers having a higher crystallization rate than the crystallization rate of PET can be solidified into a semicrystalline structure by industrial polymer processing operations such as extrusion and injection molding.

The authors thank Cem Kahruman and Ahmet O. Kalpaklı (Metallurgical and Materials Engineering Department, Istanbul University) for their help with the scanning electron microscopy study.

References

1. Kint, D. P. R.; Munoz-Guerra, S. Polym Int 2003, 52, 321.
2. Supabhol, P.; Dangseeyun, N.; Srimoaon, P.; Nithitanakul, M. Thermochim Acta 2003, 406, 207.
3. Dangseeyun, N.; Srimoaon, P.; Supaphol, P.; Nithitanakul, M. Thermochim Acta 2004, 409, 63.
4. Chisholm, B. J.; Zimmer, J. G. J Appl Polym Sci 2000, 76, 1296.
5. Palys, L. H.; Phillips, P. J. J Polym Sci Polym Phys Ed 1980, 18, 829.
6. Xanthos, M.; Baltzis, B. C.; Hsu, P. P. J Appl Polym Sci 1997, 64, 1423.
7. Bian, J.; Ye, S. R.; Feng, L. X. J Polym Sci Part B: Polym Phys 2003, 41, 2135.
8. Mitra, D.; Misra, A. J Appl Polym Sci 1988, 36, 387.
9. Yu, Y.; Yu, Y.; Jin, M.; Li, G.; Bu, H. Macromol Chem Phys 2001, 202, 139.
10. Wu, T. M.; Chang, C. C.; Yu, T. L. J Polym Sci Part B: Polym Phys 2000, 38, 2515.
11. Lee, B.; Lee, J. W.; Lee, S. W.; Yoon, J.; Ree, M. Polym Eng Sci 2004, 44, 1682.
12. Kong, X.; Yang, X.; Zhou, E.; Ma, D. Eur Polym J 2000, 36, 1085.
13. Kong, X.; Yang, X.; Li, G.; Zhao, X.; Zhou, E.; Ma, D. Eur Polym J 2001, 37, 1855.
14. Li, W.; Kong, X.; Zhou, E.; Ma, D. Polymer 2005, 46, 11655.
15. Xiao, J.; Zhang, H.; Wan, X.; Zhang, D.; Zhou, Q.; Woo, E. M.; Turner, S. R. Polymer 2002, 43, 3683.
16. Agarwal, U. S.; de Wit, G.; Lemstra, P. J. Polymer 2002, 43, 5709.
17. Zhang, Y.; Gu, L. Eur Polym J 2000, 36, 759.
18. Garlotta, D. J Polym Environ 2002, 9, 63.
19. Acar, I.; Kaşgöz, A.; Özgümüş, S.; Orbay, M. Polym-Plast Tech Eng 2006, 45, 351.
20. Acar, I. Ph.D. Thesis, Istanbul University, 2003.
21. Güçlü, G.; Yalçınyuva, T.; Özgümüş, S.; Orbay, M. Thermochim Acta 2003, 404, 193.
22. Papageorgiou, G. Z.; Achilias, D. S.; Bikiaris, D. N.; Karayannidis, G. P. J Therm Anal Calorim 2006, 84, 85.
23. Yu, Y.; Bu, H. Macromol Chem Phys 2001, 202, 421.
24. Yu, Y.; Yu, Y.; Jin, M.; Bu, H. Macromol Chem Phys 2000, 201, 1894.
25. Bouma, K.; de Wit, G.; Lohmeijer, J. H. G. M.; Gaymans, R. J. Polymer 2000, 41, 3695.
26. Ozawa, T. Polymer 1971, 12, 150.
27. Cebe, P.; Hong, S. D. Polymer 1986, 27, 1183.
28. Addonizio, M. L.; Martuscelli, E.; Silvestre, C. Polymer 1987, 28, 183.
29. Avrami, M. J Chem Phys 1939, 7, 1103.
30. Avrami, M. J Chem Phys 1940, 8, 212.
31. Avrami, M. J Chem Phys 1941, 9, 177.
32. Jeziorny, A. Polymer 1978, 19, 1142.
33. An, Y.; Dong, L.; Mo, Z.; Liu, T.; Feng, Z. J Polym Sci Part B: Polym Phys 1998, 36, 1305.
34. Kissinger, H. E. J Res Natl Bur Stand 1956, 57, 217.
35. Lu, X. F.; Hay, J. N. Polymer 2001, 42, 9423.
36. Wang, Z. G.; Hsiao, B. S.; Sauer, B. B.; Kampert, W. G. Polymer 1999, 40, 4615.
37. Zhou, C.; Clough, S. B. Polym Eng Sci 1988, 28, 65.
38. Blundell, D. J.; Osborn, B. N. Polymer 1983, 24, 953.